Sources and sinks of dissolved inorganic carbon in an urban tropical coastal bay revealed by δ13C-DIC signals

Luiz Cotovicz, Bastiaan Knoppers, Loris Deirmendjian, Gwenaël Abril

1   Sources and sinks of dissolved inorganic carbon in an urban tropical coastal bay revealed by δ^{13}C-
2   DIC signals

3   Luiz C. Cotovicz Jr.[*,a,b]; Bastiaan A. Knoppers[a]; Loris Deirmendjian[b]; Gwenaël Abril[a,b,c]

4

5   [a] Programa de Geoquímica, Universidade Federal Fluminense, Niterói, RJ, Brazil

6   [b]Laboratoire, Environnements et Paléoenvironnements Océaniques et Continentaux (EPOC)
7   UMR 5805, CNRS – Université de Bordeaux – Pessac, France

8   [c] Biologie des Organismes et Ecosystèmes Aquatiques (BOREA), UMR 7208, Muséum National
9   d'Histoire Naturelle, CNRS, SU, UCN, UA, IRD, 61 rue Buffon, 75231, Paris cedex 05, France.

10   * Corresponding author: lccjunior@id.uff.br

11

12

13

14

15

16

17

18

19

20

21

22

23

24

25

26

27

28

29

30

31   Abstract

32   Dissolved inorganic carbon (DIC), its stable isotope composition (δ^{13}C-DIC) and ancillary
33   parameters of the water column were investigated in a eutrophic tropical marine-dominated
34   estuary surrounded by a large urban area (Guanabara Bay, Rio de Janeiro, Brazil). Most negative
35   δ^{13}C-DIC signatures (down to -6.1‰) were found in polluted regions affected by direct sewage
36   discharges where net heterotrophy induces high partial pressure of CO_2 (pCO$_2$) and DIC
37   concentrations. Keeling plot was applied to this polluted region and determined the δ^{13}C-DIC
38   sewage signature source of -12.2‰, which is very consistent with isotopic signature found in
39   wastewater treatment plans. These negative δ^{13}C-DIC signatures (i.e., DIC depleted in ^{13}C) were
40   restricted to the vicinity of urban outlets, whereas in the largest area of the bay δ^{13}C-DIC
41   signatures were more positive (i.e., DIC enriched in ^{13}C). The most positive δ^{13}C-DIC signatures
42   (up to 4.6‰) were found in surface waters dominated by large phytoplankton blooms, with
43   positive correlation with chlorophyll a (Chl a). In the largest area of the bay, the preferential
44   uptake of the lighter stable carbon isotope (^{12}C) during photosynthesis followed the Rayleigh
45   distillation, and appeared as the most important driver of δ^{13}C-DIC variations. This reveals an
46   important isotopic fractionation (ε) by phytoplankton due to successive algal blooms that has
47   turned the remaining DIC pool enriched with the heavier stable carbon isotope (^{13}C). The
48   calculated diel apparent ε showed higher values in the morning (18.7‰ to 21.6‰) and decreasing
49   in the afternoon (6.8‰ to 11.1‰). ε was positively correlated to the pCO$_2$ ($R^2 = 0.88$, p = 0.005)
50   and DIC concentrations ($R^2 = 0.73$, p = 0.02), suggesting a decline in carbon assimilation
51   efficiency and decreasing uptake of the lighter carbon under CO_2 limiting conditions. The
52   eutrophic coastal waters of Guanabara Bay have δ^{13}C-DIC signatures well above that found in
53   estuaries, shelf and ocean waters worldwide.

54   Keywords: δ^{13}C-DIC signatures; coastal eutrophication; carbon cycling; Guanabara Bay

1. Introduction

The coastal zone is one of the most biologically active areas of the biosphere, and plays an important role in the global carbon cycle (Gattuso et al. 1998). Estuaries are considered prominent coastal environments, which receive large amounts of organic matter from land, and exchange material with the adjacent ocean and the atmosphere (Borges and Abril, 2011; Chen et al. 2013). The most recent global estimation of estuarine CO_2 emissions to the atmosphere is about 0.1 Pg C yr^{-1} (Chen et al. 2013). These emissions occur because in estuaries the consumption of organic carbon exceeds net primary production, and the net heterotrophy in the ecosystem leads to high pCO_2 levels (Gazeau et al. 2004; Borges and Abril, 2011), together with lateral CO_2 inputs from tidal wetlands (Cai and Wang 1998., Bouillon et al. 2003; Bouillon et al. 2011) and rivers (Frankignoulle et al. 1998; Hunt et al. 2011; Joesoef et al. 2017). However, it must be highlighted that the high diversity of estuarine morphological types and associated ecosystems creates strong local and regional differences that hinders the extrapolation of results for global estimations, which remain uncertain (Borges, 2005).

The δ^{13}C-DIC is a helpful tool understanding biogeochemical cycling and tracing the sources, sinks and transformations of carbon in aquatic ecosystems (Gillikin et al. 2006; Burt et al. 2016). During photosynthesis, plants use preferentially the lighter stable carbon isotope (^{12}C) than the heavier stable carbon isotope (^{13}C). This carbon stable isotope discrimination leads to an isotopic fractionation and, thus, organic carbon in marine plants and algae are depleted in ^{13}C relative to their DIC source (Burkhardt et al. 1999). Therefore, aquatic primary production tends to leave the water rich in ^{13}C, increasing δ^{13}C-DIC signatures (Zeebe and Wolf-Gladrow, 2001). On the other hand, the degradation of organic carbon by respiring heterotrophic organisms, either in pelagic or in benthic compartments, produces CO_2 with approximately the same isotopic signature of the respired organic matter, decreasing δ^{13}C-DIC signatures (Kendall and Doctor, 2004; Miyajima et al. 2009; Bouillon et al. 2011; Bhavya et al. 2018).

The freshwater δ^{13}C-DIC endmember in estuaries could present very different values, and related to distinct isotopic signatures from the major sources and sinks, including biogenic and lithological sources, air-water CO_2 exchanges, and *in situ* metabolism (Mook and Tan, 1991; Campeau et al. 2017). This large heterogeneity leads to freshwater end-members generally ranging between -5‰ and -25‰, depending on the intensity of the different δ^{13}C-DIC sources and sinks (Kendall and Doctor, 2004; Finlay and Kendall, 2007). This results in marked changes in the stable isotope carbon composition across estuarine salinity gradients from freshwater to the sea (Fry, 2002). Very negative δ^{13}C-DIC signatures (down to – 20‰ or range), which shows a strong depletion of ^{13}C in the DIC pool, were documented in several estuaries, especially at low salinity regions, which are usually highly heterotrophic (Bouillon et al. 2007; Bouillon et al. 2011). Contrary to low salinity regions, the marine-dominated regions of estuaries exhibit higher δ^{13}C-DIC signatures that are usually in the range of -2‰ to +2‰ (mean approaching 0‰) due to a predominance of marine DIC and a limited influence of DIC from terrestrial sources (Mook and Tan, 1991; Chanton and Lewis, 1999; Gruber et al. 1999). Generally, the stable isotope signature of DIC in estuaries follows mixing process between marine and freshwater end-members (Mook and Tan, 1991), attesting that DIC levels are mainly controlled by physical processes (Wang et al. 2016). However, deviation from mixing curves are frequently reported (Coffin and Cifuentes, 1999; Bouillon et al. 2003; Gillikin et al. 2006; Miyajima et al. 2009; Bouillon et al. 2011; Bhavya et al. 2018). The δ^{13}C-DIC data below conservative mixing suggest prevalence of respiration that adds depleted δ^{13}C-DIC (Bouillon et al. 2003; Bouillon et al. 2011). On the other hand, in estuaries with important levels of photosynthesis, deviation above to the mixing curve can occur due to the

101   preferential uptake of the lighter stable carbon isotope (Coffin and Cifuentes, 1999; Zeebe and
102   Wolf-Gladrow, 2001; Gillikin et al. 2006). In addition to the metabolic controls (respiration and
103   photosynthesis), the δ^{13}C-DIC dynamic is also affected by physical controls such as the CO_2
104   exchange with the atmosphere and dissolution/precipitation of carbonate minerals (Finlay and
105   Kendall, 2007). It is important to point out that when DIC reaches the equilibrium with
106   atmospheric CO_2 concentrations, the δ^{13}C-DIC becomes close to the value of 0‰ (Bouillon et al.
107   2011). However, there is an important temperature-dependent equilibrium isotope fractionation
108   of δ^{13}C-DIC (Zhang et al. 1995), and this can causes regional deviations from 0‰ depending on
109   aquatic and atmospheric temperatures.

110   In addition to the high natural variability of δ^{13}C-DIC values in estuaries and coastal zones, the
111   isotopic signature of the DIC can change in response to anthropogenic forcing (Finlay and
112   Kendall, 2007; Yang et al. 2018). Human activities, such as land-use changes, wastewater
113   discharges, and wetlands destruction, are altering carbon sources, sinks, cycling and budgets
114   (Bauer et al. 2013). Although the use of δ^{13}C-DIC is well established for investigations of
115   ecosystem metabolism and water mixing processes in estuaries, this parameter has been rarely
116   used to describe the occurrence of anthropogenic perturbations such as eutrophication. In the
117   tropics, the development of coastal megacities with inefficient treatment of wastewaters,
118   combined with enhanced biological activity due to specific climatic features, leads to drastic
119   modifications of the regional carbon cycle (Carreira et al. 2002; Cotovicz et al. 2015), which
120   should impact the isotopic signature of the DIC. Here, we present the first measurements of δ^{13}C-
121   DIC in a tropical coastal embayment that receives large amounts of untreated wastewaters from
122   surrounding urban areas, which hosts a population of about 9 millions of inhabitants. Large inputs
123   of domestic effluents into the bay enhanced the levels of aquatic primary production (Rebello et
124   al. 1988), and turned the bay into a marked sink of CO_2 (Cotovicz et al. 2015). We hypothesized
125   that these human perturbations of the estuarine system will have important impacts on the isotopic
126   signature of the DIC that need a detailed characterization. We also expected uncommon isotopic
127   signatures of these coastal waters compared to other estuarine and marine environments.

128

129   **2. Materials and Methods**

130   2.1. Study Area

131   Guanabara Bay (22°41–22°58 S and 43°02–43°18 W) is a tropical coastal embayment located at
132   the SE-Brazilian coast (Fig. 1). The surface area is 384 km^2, the mean depth is 5.7 m, and the
133   water volume is about 1870 x 10^6 m^3. The bay has a microtidal regime, and is a partially mixed
134   estuary (Kjerfve et al. 1997), but under conditions of high solar incidence and high freshwater
135   discharge the bay could present a strong vertical thermohaline stratification (Cotovicz et al. 2015).
136   The annual freshwater inputs by the rivers is only about 100 m^3 s^{-1} (Kjerfve et al. 1997). The large
137   difference between the high water volume and the low amount of freshwater inputs are reflected
138   in high salinities along the Bay (averaging 29.5 ± 4.8), with few lower values (down to 15) at the
139   vicinity of the small river mouths. Considering the bay as a whole, more than 85% of the water
140   volume corresponds to seawater, whereas only 15% is attributed to freshwaters (Costa-Santos,
141   2015). The average time necessary to renew 50% of the total water volume with the tidal
142   movements is 11.4 days, but with significant spatial differences, especially at the most confined
143   regions (Kjerfve et al. 1997). Guanabara Bay is located in the intertropical zone, and the climate
144   is characterized by a warm and wet summer, and a cooler and drier winter (Bidone and Lacerda,

145　2004). The annual freshwater input to the bay is approximately 100 ± 59 m^3 s^{-1}, and modest
146　compared to the bay's water volume, which contributed to the predominance of polyhaline to
147　euhaline waters. The bay is one of the most polluted coastal systems in the world that receives
148　large inputs of untreated domestic and industrial effluents at approximately 25 m^3 s^{-1} (Kjerfve et
149　al. 1997; Bidone and Lacerda, 2004). We compartmentalized the bay into five domains (sectors
150　1, 2, 3, 4, and 5) as described by Cotovicz et al. (2015; 2018a) for the treatment, computations
151　and interpretation of the data (Fig. 1).

152　2.2. Experimental Design, Sampling Procedures and Laboratory Analysis

153　In 2013 and 2014, nine sampling campaigns were conducted for the analysis of δ^{13}C-DIC and
154　ancillary parameters of the water column in Guanabara Bay. The water parameters were sampled
155　in continuous on-line and/or discrete procedures. Continuous measurements were performed to
156　analyze the water temperature, salinity, DO and pCO$_2$, as described by Cotovicz et al. (2015).
157　Briefly, one submersible water pump was positioned at the side of the boat (depth of 0.5 m),
158　providing continuous water flow to a measurement system located inside the boat. The continuous
159　measurements of pCO$_2$ followed the equilibration technique using a marble-type equilibrator
160　coupled to a non-dispersive infrared gas detector (LICOR 820) (Frankignoulle et al. 2001;
161　Cotovicz et al. 2016a). The equilibrator had a response time lower than 4 minutes, and, as the
162　boat speed during measurements was about 6 km h^{-1}, pCO$_2$ measurements were averaged over
163　approximately 300m of the boat's track. One calibrated YSI 6600 V2 multiparameter probe
164　measured continuously the water temperature, salinity and DO.

165　Discrete water samples were taken for δ^{13}C-DIC, chlorophyll a (Chl a), pheo-pigments, total
166　alkalinity (TA), and dissolved inorganic phosphorus (PO$_4^{3-}$), accounting to about 16-19 stations
167　distributed across the bay, except in December 2013, when only 8 stations could be sampled. Sub-
168　surface water samples were collected at 0.5 m depth with a Niskin bottle, and conditioned (i.e.
169　fixed and/or kept on ice in the dark) for further chemical analysis at the laboratory. The
170　comparison between surface and bottom waters in terms of δ^{13}C-DIC concentrations and other
171　physico-chemical parameters were performed at some stations, during the summer period, and
172　during conditions of maximal vertical stratification at summer period in sectors 3, 4, and 5
173　(Cotovicz et al. 2016b).

174　The water was filtered with whatman GF/F glass-fibre filters (porosity 0.45 µm) followed by
175　determination of suspended particulate material (SPM), Chl a and pheo-pigments. The filters were
176　pre-combusted (at 500° C during 6 hours) and pre-weighted before utilization. After filtration,
177　filters were dried in an oven at 50°C and then weighed. SPM was determined gravimetrically. Chl
178　a and pheo-pigments were extracted in 90% acetone and quantified spectrophotometrically before
179　and after acidification of the samples, according to Strickland and Parsons (1972). PO$_4^{3-}$ was
180　quantified by the colorimetric method as in Grasshoff et al. (1999). For the stable isotope
181　composition of the DIC, the water was sampled and transferred directly to 150 mL serum vials,
182　which were poisoned by adding 0.2 mL of a solution saturated with HgCl$_2$ and carefully sealed,
183　taking care that no air remained in contact with samples. Vials were also stored in the dark to
184　prevent photo oxidation. In the laboratory, the δ^{13}C-DIC signature was determined following the
185　protocol of Bouillon et al. (2007). We injected 40 mL of helium gas inside the bottles to create a
186　headspace, maintaining the bottles bottom-up and simultaneously expelling water by a second
187　needle.. Then, 0.2 mL of ultrapure and concentrated H$_3$PO$_4$ was introduced to convert all
188　inorganic carbon to CO$_2$. Samples were shaken vigorously and kept 12h in the dark at a controlled
189　temperature of 25°C. The δ^{13}C of CO$_2$ in the headspace was determined by injecting between 0.5

190 mL and 1 mL of the headspace gas in an isotopic ratio mass spectrometer (IRMS, Micromass
191 IsoPrime), equipped with a manual gas injection port. $\delta^{13}C$-DIC was calibrated using a laboratory
192 standard, which was prepared adding 45 mg of Na_2CO_3 in a sealed vial flushed with helium and
193 dissolved with 3 mL of 85% H_3PO_4, as described in Deirmendjian and Abril (2018). This standard
194 was calibrated against certified standard (NBS19, -1.96‰) using a dual-inlet IRMS. The isotopic
195 value of the Na_2CO_3 standard was -4.5±0.2‰. The obtained $\delta^{13}C$ values were corrected for the
196 partitioning of CO_2 between the gaseous (headspace) and water phase in each sample using the
197 algorithm of Miyajima et al. (1995). The repeatability of the analysis was approximately 0.1‰.
198 The $\delta^{13}C$-DIC signatures are reported in ‰ relative to the standard Vienna Pee Dee Belemnite
199 (V-PDB) scale. TA was measured on 70 mL of filtrate samples, by the classical Gran titration
200 method (Gran, 1952) using an automated titration system (Mettler Toledo model T50). The
201 reproducibility of the titration was ± 3 $\mu mol\ kg^{-1}$ (n = 5), and the accuracy was estimated at ± 5
202 $\mu mol\ kg^{-1}$ (inferred from certified material reference, CRM, provided by A. G. Dickson, Scripps
203 institution of Oceanography). To compare the pCO_2 with discrete sampling, we used the value of
204 pCO_2 exactly the moment of the discrete sampling at the fixed station (after achievement of
205 equilibration). As such, we obtained the values of pCO_2 and TA at same time and place. DIC
206 concentrations were calculated from the values of pCO_2 and TA, and were very consistent with
207 the DIC calculated from the values of measured pH and TA (Cotovicz et al. 2015). Calculations
208 of DIC were made using the carbonic acid constants proposed by Mehrbach et al. (1973) refitted
209 by Dickson and Millero (1987) as implemented in the CO2Calc V 4.0.9 program (Robbins et al.
210 2010).

211

212 2.3. Calculation of DIC and $\delta^{13}C$-DIC addition or loss

213 Guanabara Bay did not present a marked saline gradient (Tab. 1; range was 14 to 35). Instead,
214 this bay presents salinities generally higher than 30, and the low salinity waters are restricted to
215 locations close to the river water and effluent discharges. When the river DIC inputs are weak or
216 negligible, the conservative mixing of DIC (DIC_{mixing}) can be calculate using the marine end-
217 member as follows (Jiang et al. 2008):

218 $DIC_{mixing} = S_i/S_{ocean}*DIC_{ocean}$ (1)

219 Where S_i is the measured salinity, S_{ocean} the salinity of the ocean end-member, and DIC_{ocean} the
220 DIC concentration of the ocean end-member. The DIC_{mixing} is the DIC concentration after the
221 ocean end-member is diluted by a zero DIC freshwater; however, this equation also includes
222 possible DIC inputs from river (Jiang et al. 2008).

223 The excess of DIC (ΔDIC_{excess}) is defined as the DIC addition or loss relative to the conservative
224 mixing (Jiang et al. 2008), and can be expressed as:

225 $\Delta DIC_{excess} = DIC_i - DIC_{mixing}$ (2)

226 Where DIC_i is the measured DIC. In the same way, the excess of total alkalinity (ΔTA_{excess}) can
227 be calculated as the deviation from the conservative mixing:

228 $\Delta TA_{excess} = TA_i - TA_{mixing}$ (3)

229 In a similar approach developed by Yang et al. (2018), the difference between the $\delta^{13}C$-DIC of
230 the sample ($\delta^{13}C$-DIC_i) and the $\delta^{13}C$-DIC of the marine end-member ($\delta^{13}C$-DIC_{ocean}) represent the

231   stable isotopic deviation from the marine end-member ($\Delta\delta^{13}$C-DIC) linked to local processes, as
232   follows:

233     $\Delta\delta^{13}$C-DIC = δ^{13}C-DIC$_i$ - δ^{13}C-DIC$_{ocean}$ (4)

234   When DIC is altered by processes of organic carbon degradation, primary production, and/or air-
235   water exchanges, its isotopic composition is also altered, following mass balance equations
236   (complete set of equation can be found in Yang et al. 2018). The simplified equation is:

237     $\Delta\delta^{13}$C-DIC = ΔDIC$_{excess}$/DIC$_i$*(δ^{13}C$_{excess}$-δ^{13}C$_{ocean}$)   (5)

238   The δ^{13}C$_{excess}$ represent the stable isotopic composition of the added or lost DIC whereas the
239   δ^{13}C$_{ocean}$ is the stable isotopic composition of the marine end-member. In coastal waters with
240   limited river inputs, the DIC$_i$ and DIC$_{ocean}$ are approximately the same. Then, the equation 5 can
241   be adjusted to:

242     $\Delta\delta^{13}$C-DIC = ΔDIC$_{excess}$/DIC$_{ocean}$*(δ^{13}C$_{excess}$-δ^{13}C$_{ocean}$)   (6)

243   This equation above means that ΔDIC$_{excess}$/DIC$_{ocean}$ and $\Delta\delta^{13}$C-DIC are linked and linearly related.
244   In this way, the slope of this relationship can be used to infer the isotopic composition of the
245   added or lost DIC and the ocean end-member value (Yang et al. 2018).

246   The δ^{13}C signature of the added or lost DIC due to the organic carbon production or respiration
247   was taken as the average of δ^{13}C-POC value in the bay, which is about -20‰ (Kalas et al. 2009).
248   The fractionation factor (αCO$_2$) due to outgassing of CO$_2$ was calculated following the procedures
249   described by Alling et al. (2012) and Samanta et al. (2015). We applied the equation of Rau et al.
250   (1996) to estimate the fractionation factor (α) between DIC and the dissolved CO$_2$ in water,
251   according to:

252   δ^{13}C-CO$_2$ = δ^{13}C-DIC + 23.644 – 9701.5/T   (7)

253   This equation gives the equilibrium fractionation factor (ϵCO$_2$), which is the difference between
254   δ^{13}C-CO$_2$ and δ^{13}C-DIC. This calculation provides a value of ϵCO$_2$ of -9.2‰, representing the
255   averaged found in the sector 2 (the only sector that is a net source of CO$_2$ to the atmosphere).
256   Defining fCO$_2$ as the fraction of DIC remaining in the water after outgassing of CO$_2$, we can
257   calculate the DIC concentration after CO$_2$ loss (DIC$_F$, which is equivalent to the measured DIC,
258   DICi), according:

259   DIC$_F$ = fCO$_2$ * DIC$_I$ (8)

260   where DIC$_I$ represents the initial DIC concentration before outgassing, which is equivalent to the
261   calculated DIC based on equation 1, DIC$_{mixing}$. The ^{13}C/^{12}C ratio in the remaining waters (R$_F$) will
262   be fractionated during progressive outgassing by the Rayleigh distillation process, according:

263   R$_F$= R$_I$ (fCO$_2$) $^{\alpha CO2-1}$ (9)

264   Where R$_I$ is the initial ^{13}C/^{12}C ratio before outgassing. This equation is equivalent to (Alling et al.
265   2012):

266   δ^{13}C$_F$ = δ^{13}C$_I$ + 10^3 (α_{CO2} - 1) ln(f$_{CO2}$)   (10)

267   If we consider that the amount of DIC that is lost by outgassing is small compared to the total
268   pool of DIC (Alling et al. 2012; Samanta et al. 2015), the DIC_F tend to be close to DIC_{mixing} (in
269   fact this ratio is close to 1 in Guanabara Bay, and consistent with other studies). In this way,
270   equations 1, 4, 8 and 9 can be combined:

271     $\Delta\delta^{13}C\text{-}DIC \sim \Delta DIC_{exccess}\,(\alpha_{CO2} - 1)10^3$ (11)

272   Considering that $\alpha CO_2 \sim 0.991$ in Guanabara Bay, there is a near linear relationship between
273     $\Delta\delta^{13}C\text{-}DIC$ and ΔDIC_{excess}, with a slope of -9.2 value of outgassed CO_2. As the bay is a net sink
274   of CO_2 (Cotovicz et al. 2015), we also calculate a slope representing the uptake of atmospheric
275   CO_2. During uptake, $\alpha CO_2 \sim 0.998$ (Siegethaler and Münnich, 1981; Inoue and Sugimura, 1985),
276   giving a slope of approximately -2.0 that represents the process of CO_2 uptake.

277   The average $\delta^{13}C$ -DIC signature of the wastewater DIC input was calculate with the keeling plot
278   for the most polluted region (Fig. S1, supplementary file), which give a value of -12.2‰. This
279   stable isotopic signature is very consistent with that found in wastewater samples (-12.0‰).

280

281   2.4. Estimates of the apparent photosynthetic fractionation factor of DIC (ε-DIC)

282   Photosynthesis leads to the ^{13}C enrichment of the remaining DIC pool as the phytoplankton uses
283   preferentially the ^{12}C (Mook 2001). The photosynthetic fractionation factor of DIC consumed (ε_p-
284   DIC) was calculated using the diurnal variations in the DIC concentrations and its stable isotope
285   composition. In Sep.2013, Jan.2014 and Apr.2014, diurnal variations in water $\delta^{13}C\text{-}DIC$ were
286   estimated within the upper sectors (sector 4 and 5) by performing lateral trajectories back and
287   forth across the sectors from dawn to noon (further referred as morning period) and from noon to
288   dusk (further referred as afternoon period). The stable isotope composition of the DIC used by
289   phytoplankton ($\delta^{13}C_{used}$) from dawn to noon period is likened to the DIC concentrations and its
290   stable isotope composition observed between these two periods considering a simple conservative
291   mixing by a mass balance equation:

292     $\delta^{13}C_{used} = (DIC_{dawn}\delta^{13}C_{dawn}\text{-}DIC_{noon}\delta^{13}C_{noon})\,/(DIC_{dawn}\text{-}DIC_{noon})$ (12)

293   where $\delta^{13}C_{dawn}$ and $\delta^{13}C_{noon}$ refer to the stable isotope composition of the DIC at dawn and noon,
294   respectively, and DIC_{dawn} and DIC_{noon} refer to their respective concentrations. This formulation
295   was also applied to investigate the stable isotope composition of the DIC used by phytoplankton
296   during the afternoon. Then, this apparent photosynthetic fractionation of DIC (ε_p-DIC) was then
297   estimated as the difference between the initial composition of DIC ($\delta^{13}C\text{-}DIC_i$) and the calculated
298     $\delta^{13}C_{used}$ for each period (morning and afternoon), as follows:

299     $\varepsilon_p\text{-}DIC = \delta^{13}C\text{-}DIC_i - \delta^{13}C_{used}$ (13)

300   In addition, we calculated the plots of Rayleigh Distillation, where the increase in $\delta^{13}C\text{-}DIC$ was
301   plotted against the consumed DIC at the diel scale, in a similar approach of Dam et al. (2018).

302

303   2.5. Statistical Analysis

304   The Shapiro-Wilk test showed that data of pCO_2, TA, DIC, $\delta^{13}C\text{-}DIC$ and Chl a did not follow a
305   normal distribution. Consequently, non-parametric statistical tests were performed. The paired

306 Wilcoxon test was used to compare concentrations of the measured parameters between surface
307 and bottom waters. The seasonal differences were analyzed by the Mann-Whitney test. Spearman
308 rank coefficient was used to calculate the coefficient correlations between the measured
309 parameters. Linear and non-linear (second order polynomial) regressions were also calculated.
310 All statistical analysis were based on $\alpha = 0.05$ and were performed with the GraphPad Prism 6
311 software.

312 2.6. Data Compilation and Literature Survey

313 A compilation of δ^{13}C-DIC signatures from global databases such as the *Institute National des*
314 *Sciences de L'Univers* (INSU-France) and the Carbon Dioxide Information Analysis Center
315 (CDIAC) was carried out to obtain δ^{13}C-DIC data of other estuarine, coastal and open ocean
316 waters worldwide. We also used the search engines Google Scholar and Web of Science to
317 compile data from literature. We recorded the available data directly from tables and/or
318 interpolated from figures using the data extraction program PlotDigitalizer. The different δ^{13}C-
319 DIC data obtained from this compilation work were ranked according to their salinity in order to
320 compare it with the data obtained in this study.

321 3. Results

322 The Table 1 showed the average concentrations with standard deviations as well as the ranges of
323 the main water parameters analyzed in this study, separated by sectors. The upper sectors of the
324 bay (sectors 4 and 5) presented lower salinities (27 ± 4.3 and 27.2 ± 3.5, respectively) and higher
325 temperatures (26.8 ± 2.6 °C and 26.7 ± 2.2 °C, respectively), associated to waters with longest
326 residence times (Tab. 1). To the contrary of upper sectors, sector 1 which is located near the mouth
327 of the bay, showed lower temperatures (23.8 ± 1.7 °C) and higher salinities (32.2 ± 2.1) as
328 expected due to the major influence of shelf waters.

329

	Sector 1	Sector 2	Sector 3	Sector 4	Sector 5
Temperature (°C)	23.8 ± 1.7 (21.0 – 29.3)	25.5 ± 2.2 (22.1 – 32.4)	25.4 ± 2.1 (22.1 – 31.5)	26.8 ± 2.6 (22.0 – 32.3)	26.7 ± 2.2 (22.6 – 33.9)
Salinity	32.2 ± 2.1 (25.4 – 34.9)	30.3 ± 2.4 (17.7 – 33.7)	29.8 ± 3.0 (15.1 – 33.8)	27.0 ± 4.3 (14.6 – 33.2)	27.2 ± 3.5 (16.6 – 32.9)
δ^{13}C-DIC (‰)	1.59 ± 0.84 (-0.02 / 3.03)	0.43 ± 1.93 (-6.17 / 3.24)	1.68 ± 1.25 (-1.88 / 4.57)	1.15 ± 1.50 (-2.50 / 3.81)	(0.99 ± 1.66) (-4.87 / 3.71)
pCO$_2$ (ppmv)	411 ± 145 (104 – 747)	711 ± 561 (50 – 3715)	286 ± 157 (41 – 660)	307 ± 256 (29 – 2222)	272 ± 293 (22 – 2203)
pH (NBS)	8.20 ± 0.16 (7.90 – 8.71)	8.15 ± 0.32 (7.33 – 8.96)	8.35 ± 0.23 (7.88 – 8.96)	8.34 ± 0.29 (7.39 – 9.01)	8.44 ± 0.31 (7.51 – 9.23)
TA (μmol.kg^{-1})	2240 ± 92 (1942 - 2320)	2291 ± 99 (1890 - 2488)	2168 ± 177 (1507 - 2500)	2045 ± 369 (2111 - 3920)	2137 ± 166 (1479 - 2314)
DIC (μmol.kg^{-1})	1985 ± 120 (1720 - 2127)	2044 ± 268 (1526 - 2523)	1847 ± 257 (1332 - 2290)	1658 ± 259 (1095 - 2118)	1758 ± 264 (1198 - 2190)
DO (%)	103 ± 29 (48 - 221)	97 ± 59 (2 - 263)	138 ± 51 (56 - 357)	142 ± 62 (30 - 361)	160 ± 69 (46 - 370)
Chl-*a* (μg.L^{-1})	19.1 ± 22.0 (2.0 - 128.0)	46.2 ± 51.4 (3.3 - 212.9)	57.6 ± 90.0 (1.6 - 537.2)	69.2 ± 60.2 (13.1 - 288.8)	107.7 ± 101.8 (1.5 - 822.1)
PO$_4^{3-}$-P (μM)	1.11 ± 0.60 (0.11- 2.44)	5.28 ± 3.88 (0.17 - 20.79)	1.51 ± 1.07 (0.17 - 1.10)	1.10 ± 0.79 (0.03 - 2.96)	2.23 ± 2.17 (0.02 - 8.72)

330 Table 1: Mean (± standard deviation) and ranges of the principal parameters investigated in the
331 waters of Guanabara Bay, separated by sectors.

The δ¹³C-DIC signatures in Guanabara Bay did not present conservative distributions with salinity gradient (Fig. S2; supplementary file). Indeed, DIC in the bay was enriched in ^{13}C in some parts (mainly sectors 3, 4 and 5) relative to the marine end-member that presented a stable isotopic signature of 1.5‰ (Tab. 1), whereas in some restricted parts the bay showed ^{13}C depletion (mainly sector 2) (Tab. 1, Fig. 1). Spatially, the sectors 1 and 3 presented the higher averages of δ¹³C-DIC signatures, which were 1.6‰ and 1.7‰, respectively (Tab. 1). However, some extreme high values (δ¹³C-DIC > 3‰) were also present at the most shallow-confined regions of the bay (sectors 4 and 5) (Tab. 1). Sector 2, the most polluted region, presented the lowest average of δ¹³C-DIC, which was 0.4‰ (Tab. 1). Some more negative values of δ¹³C-DIC were also found in sectors 4 and 5 close to the outlet of rivers and urban sewage networks (Tab. 1; Fig. 1). Considering all sectors, the range of δ¹³C-DIC signature in the entire bay was -6.1‰ (Sector 2) to 4.6‰ (Sector 3). Temporally, the δ¹³C-DIC also showed important seasonal variations, especially between winter and summer periods (Fig. 1). Significantly (Mann-Whitney test, $p <$ 0.001), the summer period (considered the months of Apr. 2013, Jul. 2013, Aug. 2013, Sep. 2013 and Ap. 2014) presented more positive δ¹³C-DIC signatures than the winter period (Oct. 2013, Dec. 2013, Jan. 2014 and Feb. 2014). Indeed, the average signatures of δ¹³C-DIC for the entire bay in winter and summer were respectively 1.0‰ ± 1.4‰ and 1.5‰ ± 1.7‰. Moreover, the differences between surface and bottom waters for δ¹³C-DIC during summer were of high statistical significance ($p <$ 0.001; Wilcoxon test). DIC pool was significantly enriched in ^{13}C at the surface layer, as δ¹³C-DIC averaged at 1.8‰ ± 0.6‰ in surface waters and 1.2‰ ± 1.0‰ in bottom waters (Tab. S1, supplementary file).
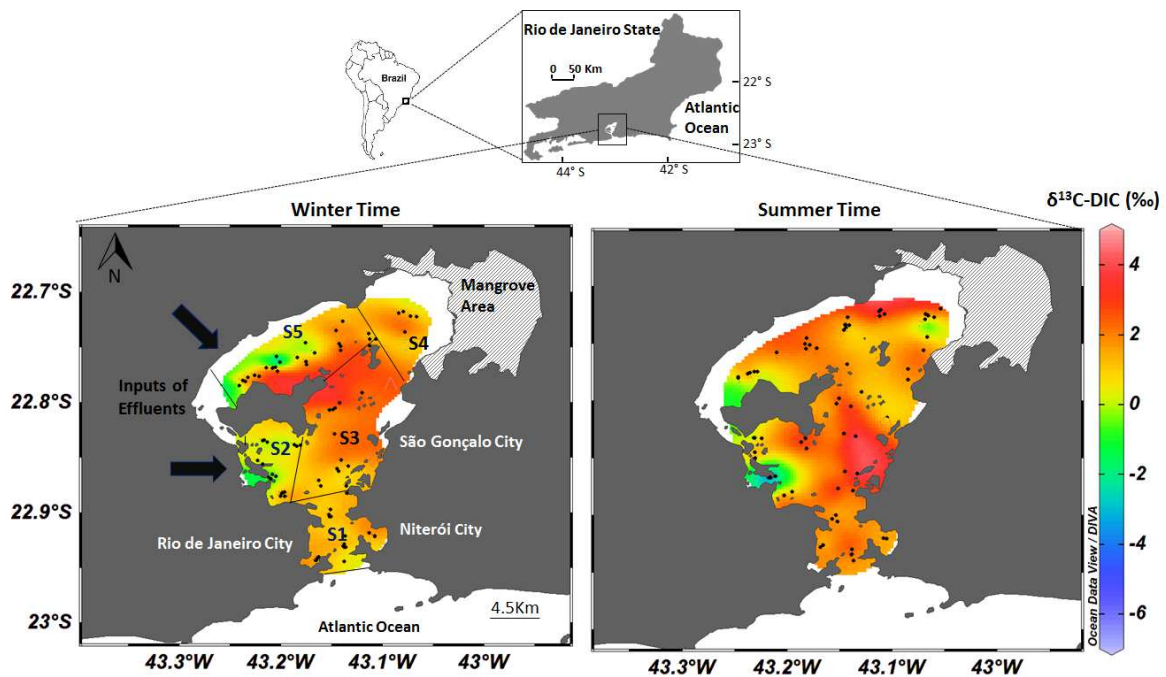

Figure 1. Composite maps showing the study area and the spatial distributions of the δ¹³C-DIC signatures in winter period (a) and summer period (b) in surface waters of the Guanabara Bay. The bay was divided into five sectors (S1 to S5). The black dots represent the sampled sites.

360   The Spearman correlation matrix was calculated for all the parameters considered in this study:
361   δ^{13}C-DIC, salinity, temperature, Chl a, DIC, pCO$_2$, DO, photosynthetically active radiation
362   (PAR), suspended particulate material (SPM), and particulate organic carbon (POC) (Tab. S2,
363   supplementary file). The values were established with averages for each sampling campaign.
364   Interestingly, δ^{13}C-DIC was significantly and positively correlated to temperature, Chl a, PAR,
365   DO, SPM and POC concentrations, while negatively correlated to pCO$_2$ levels and DIC
366   concentrations.

367   Fig. 2 showed the calculated diel photosynthetic fractionation factor (ε-DIC) plotted against the
368   discrete values of pCO$_2$ and DIC concentrations. This approach was applied only at the diel scale,
369   assuming that the phytoplankton blooms realized isotopic fractionation by incorporating
370   preferentially the lighter stable carbon isotope. We compare the fractionation between the
371   morning and the afternoon. The isotopic fractionation was higher during the morning, ranging
372   from 18.7‰ to 21.6‰ whereas lower fractionations occurred during the afternoon, and ranged
373   between 6.8‰ to 11.1‰ (Fig. 2). The photosynthetic fractionation factor was strongly and
374   positively correlated to the concentrations of DIC (R^2 = 0.73, p = 0.02) and pCO$_2$ (R^2 = 0.88, p <
375   0.005) (Fig. 2). Fig. 3 showed the plots of Rayleigh distillation that aimed to better analyze the
376   diel isotopic fractionation dynamic. The increase of δ^{13}C-DIC was related to a given change in
377   the fraction of consumed DIC. The diel cycles of production and respiration caused δ^{13}C-DIC to
378   vary between 2.1‰ and 2.8‰ (Fig. 3). The increase of δ^{13}C-DIC signatures along the day was
379   proportional to the decrease of DIC concentrations (Fig. 3). The relationship between δ^{13}C-DIC
380   and the Chl a concentrations was plotted using the sector-averaged values for each sampling
381   survey (Fig. 4). This figure shows a positive relationship between the phytoplankton biomass and
382   δ^{13}C-DIC, especially at the most productive regions of Guanabara Bay (sectors 3, 4 and 5), where
383   the extreme positive δ^{13}C-DIC signatures occurred in dense phytoplankton blooms with Chl a
384   concentrations above 50 µg L^{-1} (Fig. 4).
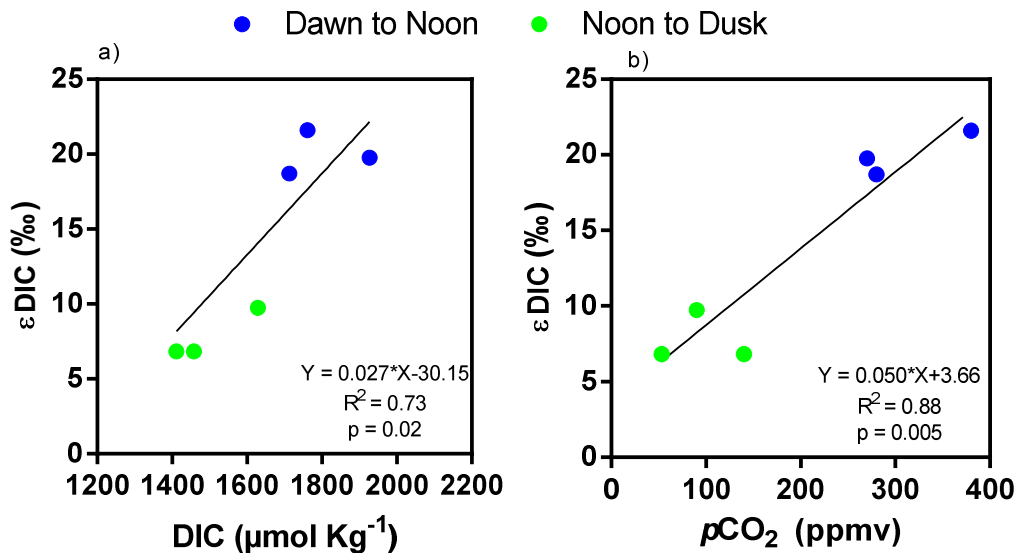
385
386   Figure 2. Calculated apparent diel phytoplankton fractionation of δ^{13}C-DIC (ε-DIC) plotted
387   against a) pCO$_2$ values and b) DIC concentrations. The blue circles represent the ε-DIC for the
388   period from dawn to noon, and the green circles represent the ε-DIC for the period from noon to
389   dusk.

390

391
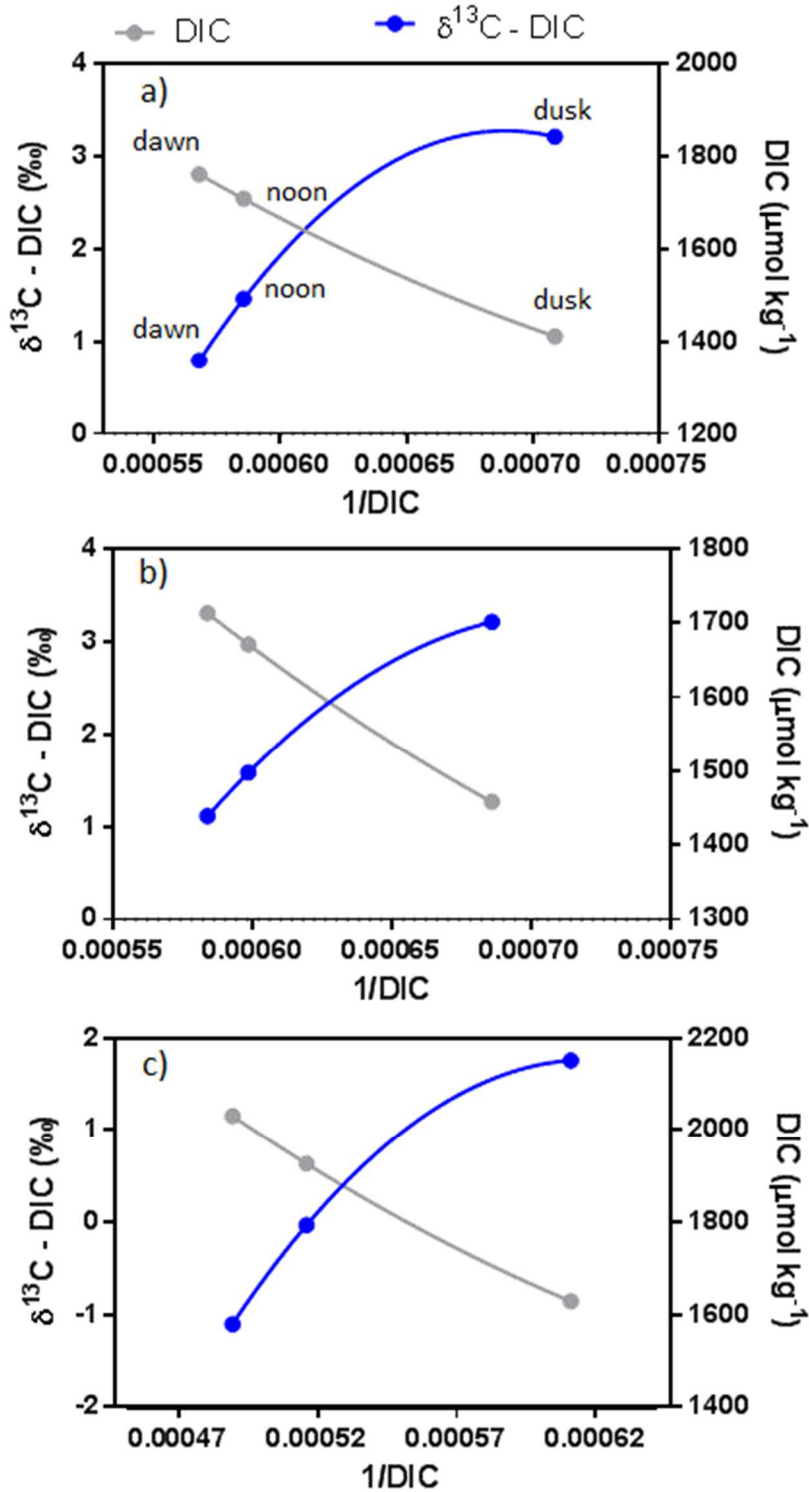
Figure 3. Plots showing the diel variations of δ13C-DIC and DIC (Rayleigh Distillation), where
the increases of δ^{13}C-DIC values are equivalent to decreases in the DIC concentrations. Graphs a,
b and c are represent the diel surveys (from dawn to dusk) in the months of Sep.2013, Jan.2014
and Apr.2014, respectively.

396
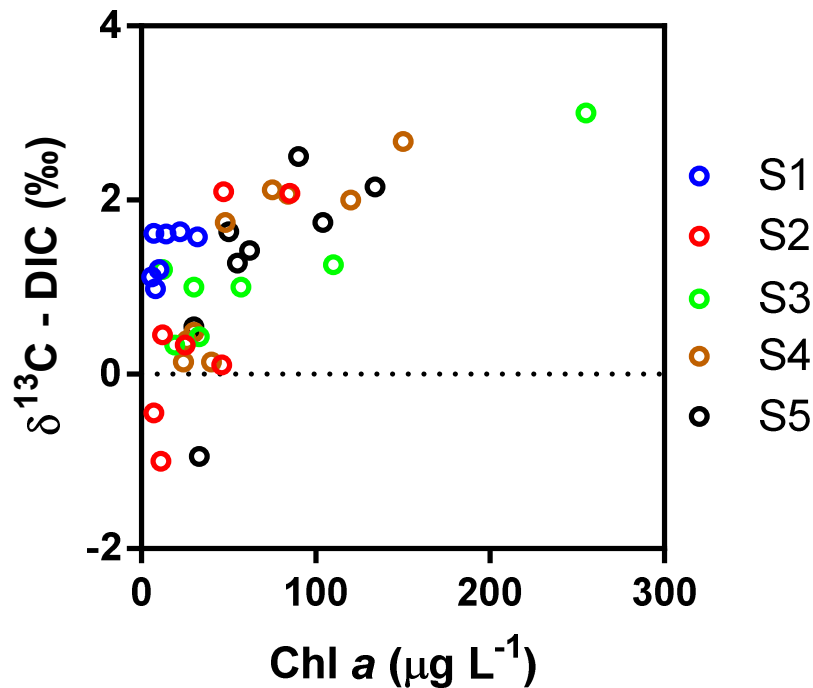
Figure 4. Relationship between δ^{13}C-DIC signatures and Chl a concentrations. The graph present the averaged-sector values for each sampling campaign.

The comparison of δ^{13}C-DIC signatures of Guanabara Bay with other ecosystems worldwide was provided in Fig. 5. Guanabara Bay showed an inverse tendency between δ^{13}C-DIC and pCO_2 values (Fig. 5a), where phytoplankton-dominated waters presented the highest δ^{13}C-DIC and the lowest pCO_2 values. The values of pCO_2 in Guanabara Bay were generally lower than the compiled data, whereas δ^{13}C-DIC signatures were much higher (Fig. 5a). This comparison of Guanabara Bay with other coastal and open ocean waters worldwide was also performed considering the salinity (Fig. 5b and 5c). These graphs showed a high scattering in the distributions of the δ^{13}C-DIC according to salinity. For a same salinity, the δ^{13}C-DIC may exhibit variation up to 20‰. The range of δ^{13}C-DIC was higher in low salinity regions and decreased progressively when freshwaters mixed with ocean waters. The salinity range between 20-30 presented the highest δ^{13}C-DIC enrichment in Guanabara Bay compared to the data from other estuaries and coasts, with a difference of about 3.20‰, on average (Fig. 5b). Compared to mangrove-dominated estuaries with salinities ranging from 15 to 20, Guanabara Bay showed an significant (Mann Whitney test, p < 0.0001) increase in δ^{13}C-DIC of 6.75‰ (Fig. 5b).
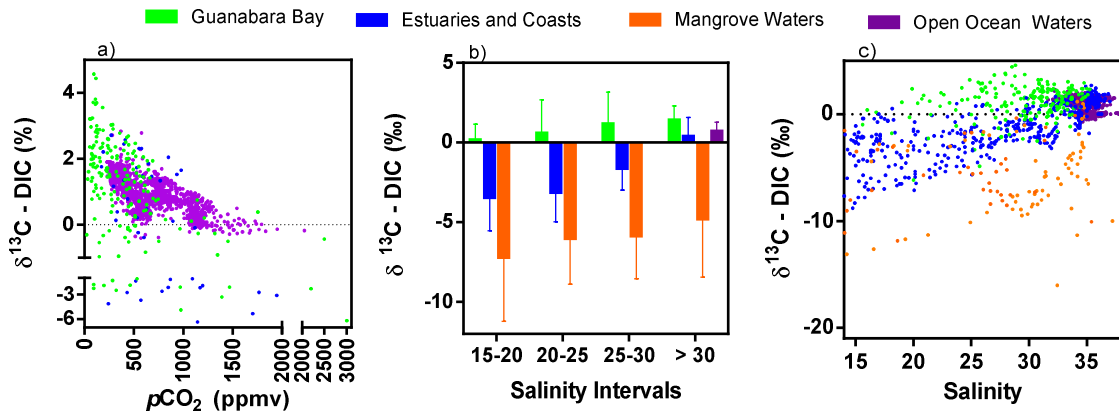
Figure 5. Comparison of Guanabara Bay with other systems worldwide: a) relationship between $\delta^{13}C$-DIC and pCO_2 values; b) distributions of $\delta^{13}C$-DIC according to salinity intervals; c) distributions of $\delta^{13}C$-DIC values against salinity. The references of the compiled data set are provided in the supplementary file.

4. Discussion

4.1 Sewage inputs of depleted $\delta^{13}C$-DIC

As a coastal embayment dominated by saline waters, the inputs of freshwater to Guanabara Bay are very low compared to its water volume (Kjerfve et al. 1997). Taking account this hydrological characteristic, we calculated the sinks and sources of DIC and TA to the system for a special case, i.e., when the freshwater inputs are weak, following the procedures described by Jiang et al. (2008). Thus, it is possible to infer the gains and losses of DIC (ΔDIC_{excess}) and TA (ΔTA_{excess}) relative to the conservative mixing (see materials and methods for details). The maximum values of ΔDIC_{excess} and ΔTA_{excess} were coincident with the highest values of pCO_2 and no related to salinity (Fig. S2; supplementary file). Oversaturation of pCO_2 in the bay was restricted to sites close to the small river mouths and sewage channels (Cotovicz et al. 2015). These polluted sites present occasional occurrence of hypoxia and anoxia events, sustaining heterotrophic metabolism (Ribeiro and Kjerfve, 2002; Cotovicz et al. 2015). Anaerobic processes including ammonification, denitrification and sulphate reduction can contributes to the production of alkalinity (Abril and Frankignoulle, 2001; Hu and Cai, 2011).

The spatial distributions of $\delta^{13}C$-DIC along Guanabara Bay shows a higher ^{13}C depletion (down to -6.17‰) only closest to the locations that receive these direct inputs of DIC from effluent discharges (Fig. 1). Fig. 6 shows the plot of $\Delta DIC_{excess}/DIC_{ocean}$ against $\Delta\delta^{13}C$-DIC, and the slopes of this relationship can be used to infer the main biogeochemical processes affecting the distributions of DIC and $\delta^{13}C$-DIC (see the figure caption for further explanations). The highest DIC additions occurred closest to Rio de Janeiro city at the northwestern region of Guanabara Bay (Sector 2). These samples from polluted sites fall within the III quadrant of the graph, indicating processes of organic carbon degradation (Samanta et al. 2015; Yang et al. 2018). For very high pCO2 values, the data in quadrant III follows the theoretical slopes of wastewater contribution (slope = -0.012; vector D) and the degradation of organic carbon (slope = -0.020; vector C), and confirms the DIC inputs more depleted in ^{13}C. These polluted regions present the

447 highest bacterial and virus contents (Fistarol et al. 2015), are sources of CO_2 and CH_4 (Cotovicz
448 et al. 2015; 2016b), and show episodic evidence of corrosive waters with low saturation state of
449 calcium carbonates (Cotovicz at el., 2018b). Similar results were found in the urbanized temperate
450 Jiaozhou Bay-China (Yang et al.; 2018), where the authors found an important input of depleted
451 δ^{13}C-DIC in waters that receive direct discharge from wastewater plans.

452 The strong negative correlation (R^2 = 0.8; p-value<0.001) between δ^{13}C-DIC and PO_4^{3-} in sector
453 2 reinforce the role of wastewaters as the main source of PO_4^{3-} and DIC depleted in ^{13}C in this
454 region (Fig. S3; supplementary file). Studies have shown that, in general, the PO_4^{3-}-P was the
455 dominant limiting nutrient in the bay, presenting sometimes an almost depletion and related to
456 the strong phytoplankton uptake (Costa-Santos 2015; Brandini et al. 2016). The calculated
457 isotopic signature of the added DIC for the samples located in these polluted regions (excluding
458 the data with Chl a concentrations > 50 µg L^{-1}) gives a stable isotopic signature of sewage source
459 of -12.2‰ (Fig. S2). This value is very consistent with that found in wastewater treatment plants
460 in China (average of -12‰; Yang et al. 2018), and with values found in a domestic sewage
461 emissary in another region of Rio de Janeiro city (-13‰; unpublished data). Taking into account
462 this, we quantified the contribution of sewage discharges for the two most polluted regions
463 (sectors 2 and 5; Fig. 1) by applying a simple two-source mixing model (Phillips and Gregg,
464 2001). We used the value of -12.2‰ as the δ^{13}C-DIC signature of sewage source, and the value
465 of 1.5‰ as the δ^{13}C-DIC-signature source of marine source (considered the average δ^{13}C-DIC
466 signature of sector 1). The model calculated a sewage contribution of about 10% in sector 2 and
467 5% in sector 5. The depleted δ^{13}C-DIC signature from polluted sources is lost very fast in the bay,
468 confirming the sewage-derived DIC is rapidly degassed and/or assimilated by phytoplankton
469 blooms, as we will discuss in the next section of the manuscript. Important to point that the
470 degassing is a process that turns the water more enriched in the heavier carbon isotope (^{13}C), since
471 that during CO_2 emissions the lighter carbon (^{12}C) is preferentially emitted due to the kinetic
472 isotope effect.

473 Another source of DIC depleted in ^{13}C to the water column in Guanabara Bay could be the
474 mangrove forest located at the northeastern region (Fig. 1); however, we could not find a clear
475 contribution into the bay (except for one sample collected close to the region, during low tide,
476 which presented a negative δ^{13}C-DIC signature of -2.5‰). This value is very far from that found
477 in mangrove-dominated waters, for example, in a tidal creek in Gazi Bay (Kenya) where the δ^{13}C-
478 DIC values were very depleted (~ -8‰) even for salinities higher than 30 (Bouillon et al. 2007)
479 (Fig. 5). This low influence of mangrove in Guanabara Bay occurs probably because of low tidal
480 pumping related to the microtidal character of the bay (Cotovicz et al. 2018a). In addition, the
481 less ^{13}C-enriched sediments were restricted to the area very close to the mangrove forest (Carreira
482 et al. 2002).

483

484 4.2 Influence of the phytoplankton fractionation on the δ^{13}C-DIC dynamics

485 Despite the influence of wastewater contribution closest to sites that receive direct sewage
486 discharge, most of δ^{13}C-DIC values are positive, indicating an isotopic fractionation of DIC by
487 marine phytoplankton by a preferential use of ^{12}C during photosynthesis (Fig. 6). Many data
488 points follow the theoretical slope of primary production (represented by vector A) that decreases
489 the ratio $\Delta DIC_{excess}/DIC_{ocean}$ and increases the $\Delta\delta^{13}$C-DIC in the quadrant I (slope of -0.020). The
490 high incidence of PAR, especially during summer, associate with high nutrient availability and

formation of thermohaline stratification, increases the rates of primary production (Rebello et al 1988), associated with development of massive phytoplankton blooms and strong CO_2 uptake (Cotovicz et al. 2015). This uptake of DIC removes preferentially the lighter ^{12}C, enriching the waters with the heavier stable carbon isotope (Mook, 2001). Successive algal blooms could consumes more of the DIC pool, and the residual DIC becomes progressively ^{13}C-enriched due to the isotopic fractionation (Finlay and Kendall, 2007). Guanabara Bay showed persistent phytoplankton blooms in all the sampling campaigns, which spread to the entire bay and cover larger areas during summer months (Cotovicz et al. 2015). Fig. 4 corroborates this result, with a positive tendency between the $\delta^{13}C$-DIC and Chl a concentrations, suggesting that the seasonal variation of the $\delta^{13}C$-DIC signature is related to changes in the extension of the phytoplankton dominance. This feature was also reported in the Perdido Estuary (Florida, USA) during periods of higher phytoplankton production (Coffin and Cifuentes 1999), in the Scheldt Estuary (Netherlands and Belgium) when the $\delta^{13}C$-DIC showed higher signatures during phytoplankton bloom periods (Hellings et al. 2001; Gillikin et al. 2006).

Fig. 6 present some points located in the quadrant IV, which represents the carbonate dissolution. The process of carbonate dissolution consumes DIC of the water column, and adds $\delta^{13}C$ with an isotopic signature closest to that of marine carbonates (0‰), turning the waters enriched in ^{13}C relative to the conservative mixing (Alling et al. 2012). However, this process is unlikely to occur in the bay since that the values of pCO_2 in quadrant IV are low and the pH values are high (Cotovicz et al. 2018b). Actually, DIC and $\delta^{13}C$-DIC can be subjected simultaneously to more than one process and not just by a specific one (Samanta et al. 2015). This means that if one sample was subject to degradation of organic carbon (represented by quadrant III) followed by primary production (represented by quadrant I), this sample could finally be located in quadrant IV (the deviation is represented by the blue arrow, which is drawn parallel to vector A). Similarly, if a sample was subject to the DIC uptake by primary production (vector A) and thereafter occurs an intrusion of atmospheric CO_2 due to the gradient at the air-water interface (CO_2 sink, vector E), this sample could also be deviated to the quadrant IV (green arrow). The red arrow is drawn parallel to vector B, representing the effect of organic carbon degradation followed by outgassing of CO_2. This is probably occurring in samples mainly from sector 2 that are located on quadrant IV that present high values of measured pCO_2, when the outgassing could be important due to important air-water gradient of CO_2. Another example is the quadrant I, where exists two vectors (A and B), representing the slopes of biological production and outgassing, respectively. Both these processes lead to loss of DIC and increase of $\delta^{13}C$-DIC. However, the process of outgassing in these samples are unlikely since that the values of pCO_2 in this quadrant are highly under-saturated.
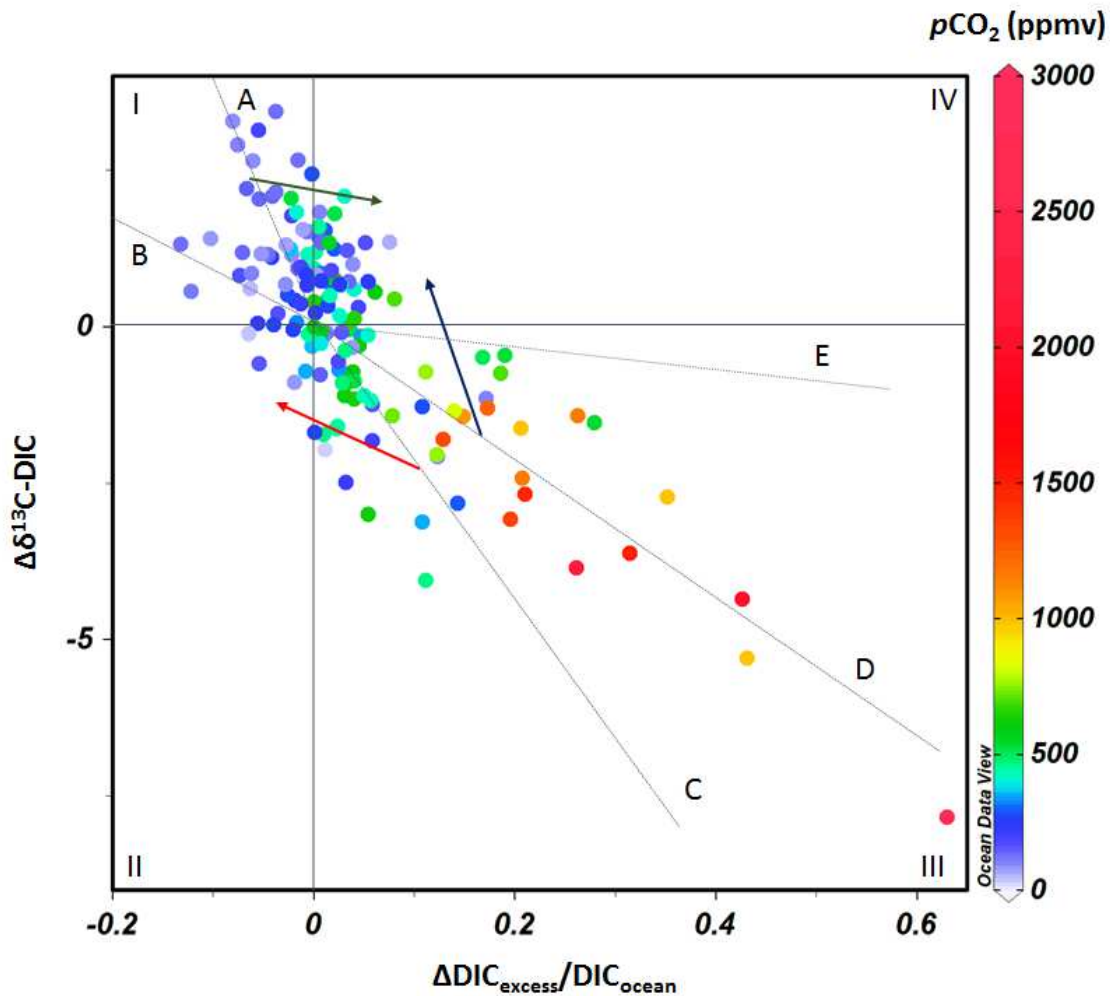
526

527

528   Figure 6. Plot of $\Delta\delta^{13}C$-DIC vs. $\Delta DIC_{excess}/DIC_{ocean}$ in the Guanabara Bay. The origin represents
529   the conservative mixing with sample values equal to the ocean end-member value (see material
530   and methods for further explanation). The four quadrants (I, II, III and IV) indicate additional
531   processes than could influence the DIC and $\delta^{13}C$-DIC distributions. The quadrant I represents the
532   primary production / outgassing of CO_2, when DIC concentrations increase and $\delta^{13}C$-DIC values
533   decrease. The quadrant II represents the calcite precipitation, when DIC concentrations and $\delta^{13}C$-
534   DIC values decrease. The quadrant III represents the degradation of organic carbon and inputs
535   from wastewater, when DIC concentrations increase and $\delta^{13}C$-DIC decrease. The quadrant IV
536   represents the carbonate dissolution, when the DIC concentrations and the vales of $\delta^{13}C$-DIC
537   increase. The vectors A, B, C, D and E represent the slopes of specific processes affecting the
538   DIC and $\delta^{13}C$-DIC distributions, that are, respectively, primary production (slope = -20.0‰), the
539   outgassing of CO_2 (slope = -9.2‰), degradation of organic carbon (slope = -20.0‰), wastewater
540   input of DIC (-12.2‰) and intrusion of atmospheric CO_2 (slope = -2.0‰). The red, blue and green
541   arrows represent the direction in which the samples will follow if they are subject to more than
542   one process. The red arrow represents the effect of organic matter degradation followed by
543   outgassing of CO_2, which is drawn parallel to vector B. The blue arrow represents the effect of
544   degradation of organic carbon followed by biological production, which is drawn parallel to
545   vector A. The green arrow represents the effect of primary production followed by intrusion of
546   atmospheric CO_2 due to the air-water gradient, which is drawn parallel to vector E.

547 The apparent phytoplankton isotopic fractionation (ε-DIC) was higher under conditions of high
548 availability of dissolved CO_2, with higher fractionation during the morning than the afternoon
549 (Fig. 2). During morning, the values of pCO_2 were higher in Guanabara Bay as the results of the
550 accumulated CO_2 respired during the nighttime (Cotovicz et al. 2015). This suggests that the
551 discrimination against ^{13}C is higher when the availability of dissolved CO_2 is higher. Previous
552 studies showed similar results, both in culture experiments (Fogel and Cifuentes, 1993), and *in
553 situ* at a Chinese hypereutrophic lake (Van Dam et al. 2018). The $\delta^{13}C$-DIC fractionation by
554 phytoplankton in Guanabara Bay follows a Rayleigh distillation (Fig. 3), where the increasing
555 removal of DIC fractions is accompanied by the isotopic fractionation of $\delta^{13}C$-DIC, turning the
556 water enriched in ^{13}C. The values of ε-DIC found during the morning period in Guanabara Bay
557 were about 20‰, a classical value for the marine phytoplankton (Fontugne and Duplessy, 1981,
558 Fogel and Cifuentes, 1999; Mook, 2001). Under conditions of low pCO_2, the $\delta^{13}C$-DIC
559 fractionation decreases during the afternoon, reflecting the decline in carbon assimilation
560 efficiency. This decrease of fractionation under CO_2 limitation was showed experimentally for
561 marine diatoms (Burkhardt et al. 1999), and it is consistent with results found in a hypertrophic
562 Chinese lake under conditions of CO_2 sub saturation (Van Dam et al. 2018). In addition, under
563 low availability of dissolved CO_2, the phytoplankton can consumes bicarbonate (HCO_3^-) (Burns
564 and Beardall, 1987), and this could contribute to decrease the isotopic fractionation factor since
565 that the isotope ratio of HCO_3^- is about 8‰ more positive than that of dissolved CO_2 (Fogel and
566 Cifuentes, 1999). Previous studies suggested an active uptake of HCO_3^- in Guanabara Bay due to
567 the enrichment of the $\delta^{13}C$-POC pool ($\delta^{13}C$-POC reaching -15.1‰; Kalas et al. 2009; Martins et
568 al. 2016). Cyanobacteria blooms, which have already been documented in Guanabara Bay, can
569 use bicarbonate under low pCO_2 availability (Miller et al. 1990).

570

571 4.3 Comparison with other ecosystems worldwide

572 The plot of $\delta^{13}C$-DIC versus pCO_2 (Fig. 5a) shows that the blooms-dominated waters present
573 strong pCO_2 under-saturation and are as well enriched in ^{13}C, that is intrinsically related to the
574 extreme levels of primary production. Guanabara Bay presented values of $\delta^{13}C$-DIC high above
575 than those of the compiled data in estuaries and coasts, revealing the advanced process of
576 eutrophication in the bay. The compiled data in estuaries presented a high scattering compared to
577 the open ocean waters, especially for values of $\delta^{13}C$-DIC lower than 0‰ (Fig. 5c). This reflects a
578 combination of processes such as respiration of terrestrial organic carbon from multiple sources
579 with different $\delta^{13}C$ signatures, weathering and the contribution of carbonate rocks in the
580 watershed, primary production, gas exchange and water mixing along the land-ocean aquatic
581 continuum (Mook, 2001). The matrix correlation (Tab. S2) shows that higher values of $\delta^{13}C$-DIC
582 are related to high levels of DO, POC, SPM, and Chl *a*, and low concentrations of DIC. Recent
583 findings in Guanabara Bay showed that the DOC and POC fractions present a large phytoplankton
584 dominance, surpassing the contribution of terrestrial sources (Cotovicz et al. 2018a). Compared
585 to other estuaries, Guanabara Bay presented the highest enrichment of ^{13}C–DIC in the salinity
586 range between 20 and 30 (Fig. 5b). In Guanabara Bay, this salinity interval is present in confined
587 stratified waters of the sectors 3, 4 and 5, which are net autotrophic and phytoplankton-dominated
588 (Rebelllo et al. 1988; Cotovicz et al. 2015; 2018a). This behavior is in contrast with most of other
589 estuarine studies, which are mostly located in temperate regions and river-dominated ecosystems,
590 where the effects of respiration, either in the water column or in sediments, are often much more
591 pronounced than photosynthesis (Mook, 2001; Bouillon et al. 2003). The relative enrichment of
592 ^{13}C–DIC is also important for salinities > 30, suggesting that Guanabara Bay can export ^{13}C-DIC

593 enriched waters to the coastal ocean. There is a marked depletion of δ^{13}C-DIC in estuaries
594 dominated by mangroves. The net inputs of ^{13}C-depleted DIC in mangroves are attributed to the
595 predominance of respiration in tidal creeks, as this process adds DIC to the water with a signature
596 similar to that of the organic matter being respired (C3 plants with signature ranging between –
597 24‰ to –30‰) (Bouillon et al. 2003; Bouillon et al. 2011; Miyajima et al. 2009).

598 In open ocean waters, the compiled data of δ^{13}C-DIC showed a range between -1.13‰ and 2.31‰,
599 averaging at 0.70‰ ± 0.57‰ (Fig. 5). This range of δ^{13}C-DIC is in accordance with previous
600 studies in seawaters with a limited influence from land carbon sources (-2‰ and 2‰; Mook and
601 Tan, 1991). However, the average of 0.71‰ is slightly lower than previous averages reported in
602 literature (Kroopnick, 1985; Mook, 2001). According to Mook (2001), the δ^{13}C-DIC in seawater
603 varies between +0‰ and +2.5‰, with the majority of data between 1‰ and 2‰. According to
604 Kroopnick (1985), the δ^{13}C-DIC of surface oceanic waters are generally around 2‰. Differences
605 in the averages and ranges of these studies can be attributed to the specific conditions during
606 sampling collection, since that consider regions with distinct biological, air-sea exchange
607 processes and different *in situ* temperatures, which could alter the δ^{13}C-DIC signature. In addition,
608 δ^{13}C-DIC could substantially differ considering the differences between surface and bottom
609 waters. δ^{13}C-DIC can present vertical stratification attributed to the oxidation of the organic
610 material produced at the surface waters (majority from phytoplanktonic origin) as it falls through
611 the water column and remineralizes at depth, with addition of isotopically light respiratory CO_2
612 to the DIC pool below the pycnocline (Kroopnick, 1985, Koné et al. 2009; Eide et al. 2017).
613 Lower δ^{13}C-DIC values in bottom waters were reported in several estuarine, coastal and open
614 ocean waters (Chou et al 2007; Burt et al 2016; Humphreys et al. 2016; Filipsson et al. 2017).
615 Guanabara Bay also present a significant vertical δ^{13}C-DIC stratification during summer, with
616 higher values at surface waters, reflecting the enrichment by phytoplankton blooms, and the
617 depletion in bottom waters due to the predominance of respiration of organic matter (Tab. S1).

618

619 5. Conclusion

620 Our results showed a strong control of δ^{13}C-DIC dynamics by biological processes in the highly
621 polluted and eutrophic Guanabara Bay. Indeed, the extreme high Chl *a* concentrations
622 concomitant with heavier δ^{13}C-DIC signatures and low pCO$_2$ values indicate a strong carbon
623 isotopic fractionation by primary production, especially at mid-inner shallow regions of the bay.
624 The isotopic fractionation induced by primary production is accentuated during summer
625 conditions when the vertical thermohaline stratification, the nutrients availability and the
626 photosynthetically active radiation were at their highest. Our calculated apparent phytoplankton
627 fractionation based on diel variations of δ^{13}C-DIC signatures and DIC concentrations showed
628 higher ^{13}C discrimination from morning to noon period, decreasing during afternoon, following a
629 Rayleigh distillation process. Overall, the *in situ* δ^{13}C-DIC concentrations were well above than
630 the values expected in equilibrium with atmospheric CO_2 concentrations. The lower/negative
631 δ^{13}C-DIC signatures were restricted to the regions under direct influence of domestic effluent
632 discharges, where high inputs of organic matter stimulate the microbial respiration that adds
633 depleted δ^{13}C-DIC into the waters. The process of air-water exchange seems also to exert
634 influence on the isotope signatures; however, in a lower magnitude compared to the biological
635 activities. Compared to the compiled data from several estuaries and open ocean waters
636 worldwide, Guanabara Bay showed a marked enrichment of ^{13}C, increasing δ^{13}C-DIC signatures.
637 The highest signature of δ^{13}C-DIC in Guanabara Bay reached 4.57‰, and to the best of our

638 knowledge, this is the highest value reported in coastal and open waters worldwide. These results
639 indicate that the eutrophication process can deeply modify the isotopic signature of the dissolved
640 inorganic carbon pool in coastal waters dominated by large algal blooms.

641

642 Acknowledgments

651

652

653

654

655

656

657

658

659

660

661

662

663

664

665

666

667

668

669

670

671 References:

672 1 Abril, G., Frankignoulle, M., 2001. Nitrogen – alkalinity interactions in the highly polluted
673 Scheldt Basin (Belgium). Water Res. 35, 844–850.

674 2 Abril, G., Richard, S., Guérin, F., 2006. In-situ measurements of dissolved gases (CH_4 and CO_2)
675 in a wide range of concentrations in a tropical reservoir using an equilibrator. Sci. Total Environ.
676 354, 246–251. https://doi.org/10.1016/j.scitotenv.2004.12.051.

677 3 Alling, V., Porcelli, D., Mörth, C. M., Anderson, L. G., Sanchez-Garcia,L., Gustafsson, Ö.
678 Andersson, P. S., Humborg, C., 2012. Degradation of terrestrial organic carbon, primary
679 production and out-gassing of CO2 in the Laptev and East Siberian Seas as inferred from δ13C
680 values of DIC, Geochim. Cosmochim. Acta. 95, 143–159,
681 https://doi.org/10.1016/j.gca.2012.07.028.

682 4 Bauer, J. E., Cai, W.-J., Raymond, P., Bianchi, T. S., Hopkinson, C. S., Regnier, P., 2013. The
683 changing carbon cycle of the coastal ocean. Nature, 504(7478), 61–70.
684 https://doi.org/10.1038/nature12857.

685 5 Bhavya, P. S., Kumar, S., Gupta, G. V. M., Sudharma, K. V., Sudheesh, V., 2018. Spatio-
686 temporal variation in $\delta^{13}CDIC$ of a tropical eutrophic estuary (Cochin estuary, India) and adjacent
687 Arabian Sea, Cont. Shelf Res., 153, 75-85, https://doi.org/10.1016/j.csr.2017.12.006

688 6 Bidone, E. D., Lacerda, L. D., 2004. The use of DPSIR framework to evaluate sustainability in
689 coastal areas, case study: Guanabara Bay Basin, Rio de Janeiro, Brazil. Reg. Environ. Change, 4,
690 5–16. https://doi.org/10.1007/s10113-003-0059-2

691 7 Borges A. V., 2005. Do we have enough pieces of the jigsaw to integrate CO_2 fluxes in the
692 coastal ocean? Estuaries. 28, 3–27. https://doi.org/10.1007/BF02732750.

693 8 Borges, A. V., Abril, G., 2011. Carbon Dioxide and Methane Dynamics in Estuaries, in:
694 Wolanski E., McLusky, D. (Eds.), Treatise on Estuarine and Coastal Science. Academic Press,
695 Amsterdam, pp. 119–161.

696 9 Bouillon, S., Frankignoulle, M., Dehairs, F., Velimirov, B., Eiler, A., Abril, G., Etcheber, H.,
697 Borges, A. V., 2003. Inorganic and organic carbon biogeochemistry in the Gautami Godavari
698 estuary (Andhra Pradesh, India) during pre-monsoon: The local impact of extensive mangrove
699 forests. Global Biogeochem. Cycles. 17. https://doi.org/10.1029/2002GB002026.

700 10 Bouillon, S., Dehairs, F., Schiettecatte, L.-S., Borges, A. V., 2007. Biogeochemistry of the
701 Tana estuary and delta (northern Kenya). Limnol. Oceanogr. 52(1), 46–59.
702 https://doi.org/10.4319/lo.2007.52.1.0046.

703 11 Bouillon, S., Connolly, R. M., Gillikin, D. P., 2012. Use of Stable Isotopes to Understand
704 Food Webs and Ecosystem Functioning in Estuaries, in: Wolanski E., McLusky, D. (Eds.),
705 Treatise on Estuarine and Coastal Science. Academic Press, Amsterdam, pp. 143–173.

706 12 Brandini, N., Rodrigues, A.P.C., Abreu, I.M., Cotovicz Jr., L.C., Knoppers, B.A., Machado,
707 W. V. 2016. Nutrient behavior in a highly-eutrophicated tropical estuarine system. Acta Limnol.
708 Bras., 28, e-21, http://dx.doi.org/10.1590/S2179-975X3416.

709   13 Burkhardt, S., Riebesell, U., Zondervan, I., 1999. Effects of growth rate, CO_2 concentration,
710   and cell size on the stable carbon isotope fractionation in marine phytoplankton. Geochim.
711   Cosmochim. Acta. 63(22), 3729–3741. https://doi.org/10.1016/S0016-7037(99)00217-3.

712   14 Burns, B.D., Beardall, J., 1987. Utilization of inorganic carbon acquisition by marine
713   microalgae. J. Exp. Mar. Biol. Ecol. 107, 75–86.

714   15 Burt, W. J., Thomas, H., Hagens, M., Pätsch J., Clargo, N. M., Salt, L. A., Winde, V., Böttcher,
715   M. E., 2016. Carbon sources in the North Sea evaluated by means of radium and stable carbon
716   isotope tracers. Limnol. Oceanogr. 61, 666–683. https://doi.org/10.1002/lno.10243.

717   16 Campeau A., Wallin, M. B., Giesler, R., Löfgren, S., Mörth, C. M., Schiff, S., Venkiteswaran,
718   J. J., Bishop, K., 2017. Multiple sources and sinks of dissolved inorganic carbon across Swedish
719   streams, refocusing the lens of stable C isotopes. Sci. Rep. 7, 1–14.
720   https://doi.org/10.1038/s41598-017-09049-9.

721   17 Carreira, R. S., Wagener, A. L. R., Readman, J. W., Fileman, T. W., Macko, S. A., Veiga, A.,
722   2002. Changes in the sedimentary organic carbon pool of a fertilized tropical estuary, Guanabara
723   Bay, Brazil: An elemental, isotopic and molecular marker approach. Mar. Chem. 79: 207– 227.
724   https://doi.org/10.1016/S0304-4203(02)00065-8

725   18 Chanton, J. P., Lewis, F. G., 1999. Plankton and Dissolved Inorganic Carbon Isotopic
726   Composition in a River-Dominated Estuary: Apalachicola Bay, Florida. Estuaries, 22(3), 575.
727   https://doi.org/10.2307/1353045.

728   19 Chen, C.-T. A., Huang, T.-H., Chen, Y.-C., Bai, Y., He, X., Kang, Y., 2013. Air–sea exchanges
729   of CO_2 in the world's coastal seas. Biogeosciences. 10, 6509–6544. https://doi.org/10.5194/bg-
730   10-6509-2013.

731   20 Chou W. C., Sheu, D. D., Lee, B. S., Tseng, C. M., Chen, C. T. A., Wang, S. L., Wong, G. T.
732   F., 2007. Depth distributions of alkalinity, TCO2 and $\delta 13C_{TCO2}$ at SEATS time-series site in the
733   northern South China Sea. Deep. Res. Part II Top. Stud. Oceanogr. 54, 1469–1485.
734   https://doi.org/10.1016/j.dsr2.2007.05.002.

735   21 Coffin, R. B., Cifuentes, L. A., 1999. Stable Isotope Analysis of Carbon Cycling in the Perdido
736   Estuary, Florida. Estuaries, 22(4), 917–926.

737   22 Costa-Santos, S. J., 2015. Determinação do estado trófico a partir da aplicação dos índices
738   O'Boyle e TRIX nos compartimentos da Baia de Guanabara, RJ. Master Dissertation, Federal
739   Fluminense University, Brazil. WWW Page,
740   https://app.uff.br/riuff/bitstream/1/1642/1/Dissertacao_Suzan%20Versao_10.1_VersaoFINAL.p
741   df

742   23 Cotovicz Jr., L. C., Knoppers, B. A., Brandini, N., Costa Santos, S. J., Abril, G., 2015. A strong
743   CO_2 sink enhanced by eutrophication in a tropical coastal embayment (Guanabara Bay, Rio de
744   Janeiro, Brazil). Biogeosciences, 12(20), 6125–6146. https://doi.org/10.5194/bg-12-6125-2015.

745   24 Cotovicz Jr., L. C., Libardoni, B., Brandini, N., Knoppers, B., Abril, G. 2016a. Comparações
746   entre medições em tempo real da pCO_2 aquática com estimativas indiretas em dois estuárioss
747   tropicais contrastantes: o estuário eutrofizado da Baia de Guanabara (RJ) e o estuário oligotrofico

748   do Rio São Francisco (AL). Química Nova, 39, 1206-1214. https://doi.org/10.21577/0100-
749   4042.20160145.22

750   25 Cotovicz Jr., L. C., Knoppers, B. A., Brandini, N., Poirier, D., Costa Santos, S. J., Abril, G.,
751   2016b. Spatio-temporal variability of methane (CH_4) concentrations and diffusive fluxes from a
752   tropical coastal embayment surrounded by a large urban area (Guanabara Bay, Rio de Janeiro,
753   Brazil). Limnol. Oceanogr., 61, S238–S252. https://doi.org/10.1002/lno.10298.

754   26 Cotovicz Jr., L. C., Knoppers, B. A., Brandini, N., Poirier, D., Costa Santos, S. J., Cordeiro,
755   R. C., Abril, G., 2018a. Predominance of phytoplankton-derived dissolved and particulate
756   organic carbon in a highly eutrophic tropical coastal embayment (Guanabara Bay, Rio de Janeiro,
757   Brazil). Biogeochemistry, 137, 1–14. https://doi.org/10.1007/s10533-017-0405-y.

758   27 Cotovicz Jr., L. C., Knoppers, B. A., Brandini, N., Poirier D., Costa Santos, S. J., Abril, G.,
759   2018b. Aragonite saturation state in a tropical coastal embayment dominated by phytoplankton
760   blooms   (Guanabara   Bay   -   Brazil).   Mar.   Pollut.   Bull.,   0–1.
761   https://doi.org/10.1016/j.marpolbul.2017.10.064.

762   28 Deirmendjian, L., Abril, G., 2018. Carbon dioxide degassing at the groundwater-stream-
763   atmosphere interface: isotopic equilibration and hydrological mass balance in a sandy watershed.
764   J. Hydrol. 558, 129-143. https://doi.org/10.1016/j.jhydrol.2018.01.003.

765   29 Dickson, A. G., Millero, F. J., 1987. A comparison of the equilibrium constants for the
766   dissociation of carbonic acid in seawater media. Deep-Sea Res. 34, 1733–1743.

767   30 Eide, M., Olsen, A. Ninnemann, U., Johannessen, T., 2017. A Global Ocean Climatology of
768   Preindustrial   and   Modern   Ocean $\delta^{13}C$,   Global   Biogeochem.   Cycles,
769   https://doi.org/10.1002/2016GB005473.

770   31 Finlay, J. C., Kendall, C., 2007. Stable isotope tracing of temporal and spatial variability in
771   organic matter sources to freshwater ecosystems, in: Michener, R., Lajtha, K. (Eds.), Stable
772   isotopes in ecology and environmental science. Blackwell Publishing, Hong Kong, pp. 594.

773   32 Filipsson, H. L., McCorkle, D. C., Mackensen, A., Bernhard, J. M., Andersson, L. S.,
774   Naustvoll, L.-J., Caballero-Alfonso, A. M., Nordberg, K., Danielssen, D. S., 2017. Seasonal
775   variability of stable carbon isotopes ($\delta^{13}CDIC$) in the Skagerrak and the Baltic Sea: Distinguishing
776   between mixing and biological productivity, Palaeogeogr. Palaeoclimatol. Palaeoecol. 483, 15-
777   30. https://doi.org/10.1016/j.palaeo.2016.11.031.

778   33 Fistarol, G. O., Coutinho, F. H., Moreira, A. P. B., Venas, T., Cánovas, A., de Paula, S. E. M.,
779   Coutinho, R., de Moura, R. L., Valentin, J. L., Tenenbaum, D. R., Paranhos, R., do Valle, R. D.,
780   Vicente, A. C. P., Amado Filho, G. M., Pereira, R. C., Kruger, R., Rezende, C. E., Thompson, C.
781   C., Salomon, P. S., Thompson F. L., 2015. Environmental and Sanitary Conditions of Guanabara
782   Bay, Rio de Janeiro. Front. Front. Microbiol., 6, 1232, https://doi.org/10.3389/fmicb.2015.01232.

783   34 Fontugne, M. R., Duplessy, J.-C., 1981. Organic carbon isotopic fractionation by marine
784   plankton in the temperature range -1 to 31°C. Oecologia Acta 4(1), 85 – 90.

785   35 Frankignoulle, M., Borges, A., Biondo, R., 2001. A new design of equilibrator to monitor
786   carbon dioxide in highly dynamic and turbid environments. Water Res. 35, 1344–1347.

787 36 Fry, B., 2002. Conservative mixing of stable isotopes across estuarine salinity gradients: A
788 conceptual framework for monitoring watershed influences on downstream fisheries production.
789 Estuaries, 25(2), 264–271. https://doi.org/10.1007/BF02691313.

790 37 Gattuso J. P., Frankignoulle, M., Wollast, R., 1998. Carbon and carbonate metabolism in
791 coastal aquatic ecosystems. Annu. Rev. Ecol. Syst. 29, 405–434.
792 https://doi.org/10.1146/annurev.ecolsys.29.1.405.

793 38 Gazeau, F., Smith, S. V., Gentili, B., Frankignoulle, M., Gattuso J.-P., 2004. The European
794 coastal zone: characterization and first assessment of ecosystem metabolism. Estuar. Coast. Shelf
795 Sci. 60(4), 673–694. https://doi.org/10.1016/j.ecss.2004.03.007.

796 39 Gillikin, D. P., Lorrain, A., Bouillon, S., Willenz, P., Dehairs, F., 2006. Stable carbon isotopic
797 composition of Mytilus edulis shells: relation to metabolism, salinity, $\delta^{13}CDIC$ and
798 phytoplankton. Org. Geochem. 37(10), 1371–1382.
799 https://doi.org/10.1016/j.orggeochem.2006.03.008.

800 40 Gran, G. 1952. Determination of the equivalence point in potentiometric titrations. Part II. The
801 Analyst, 77(920), 661-671.

802 41 Grasshoff, K., Ehrhardt, M., Kremling, K., 1999. Methods of seawater analysis. Wiley-VCH.

803 42 Gruber, N., Keeling, C. D., Bacastow, R. B., Guenther, P. R., Lueker, T. J., Wahlen, M.,
804 Meijer, H. A. J., Mook, W. G., Stocker, T. F., 1999. Spatiotemporal patterns of carbon-13 in the
805 global surface oceans and the oceanic Suess Effect. Global Biogeochem. Cycles, 13(2), 307-335.

806 43 Hellings, L., Dehairs, F., Van Damme, S., Baeyens, W. 2001. 2001. Dissolved inorganic
807 carbon in a highly polluted estuary (the Scheldt), Limnol. Oceanogr., 46(6), 1406–1414.
808 https://doi.org/10.4319/lo.2001.46.6.1406.

809 44 Hu, X., Cai, W.-J., 2011. An assessment of ocean margin anaerobic processes on oceanic
810 alkalinity budget. Glob. Biogeochem. Cycles 25, n/a. http://dx.doi.org/10.1029/2010GB003859.

811 45 Humphreys, M., Greatrix, F., Tynan, E., Achterberg, E., Griffiths, A., Fry, C., Garley, R.,
812 McDonald, A., Boyce, A., 2016. Stable carbon isotopes of dissolved inorganic carbon for a zonal
813 transect across the subpolar North Atlantic Ocean in summer 2014. Earth Syst. Sci. Data, 8, 221–
814 233. https://doi.org/ 10.5194/essd-8-221-2016.

815 46 Inoue, H. and Y. Sugimura. Carbon isotopic fractionation during the CO 2 exchange process
816 between air and sea water under equilibrium and kinetic conditions. Geochim. Cosmochim. Acta,
817 49:2453-2460, 1985.

818 47 Jiang, L. Q., Cai, W.-J., Wang, Y. C., 2008. A comparative study of carbon dioxide degassing
819 in river- and marine-dominated estuaries. Limnol. Oceanogr., 53, 2603–2615.
820 https://doi.org/10.4319/lo.2008.53.6.2603.

821 48 Kalas, F. A., Carreira, R. S., Macko, S. A., Wagener, A. L. R., 2009. Molecular and isotopic
822 characterization of the particulate organic matter from an eutrophic coastal bay in SE Brazil, Cont.
823 Shelf Res., 29, 2293–2302. https://doi.org/10.1016/j.csr.2009.09.007.

824   49 Kendall, C., Doctor, D.H., 2004. Stable isotope applications in hydrologic studies, in: Drever,
825   J.I. (Eds.), Surface and ground water, weathering, and soils: Treatise on Geochemistry, v. 5, pp.
826   319-364

827   50 Kjerfve, B., Ribeiro, C. A., Dias, G. T. M., Filippo, A., Quaresma, V. S., 1997. Oceanographic
828   characteristics of an impacted coastal bay: Baia de Guanabara, Rio de Janeiro, Brazil. Cont. Shelf
829   Res. 17, 1609–1643.

830   51 Koné Y. J. M., Abril G., Kouadio K. N., Delille B., Borges A. V., 2009. Seasonal variability
831   of carbon dioxide in the rivers and lagoons of Ivory Coast (West Africa). Estuar. Coast. 32, 246–
832   260. https://doi.org/10.1007/s12237-008-9121-0.

833   52 Kroopnick, P. M., 1985. The distribution of 13C of $\Sigma\,CO_2$ in the world oceans, Deep Sea Res.
834   Part A, Oceanogr. Res. Pap., 32(1), 57–84. https://doi.org/10.1016/0198-0149(85)90017-2.

835   53 Kubo, A., Maeda, Y., Kanda, J. 2017. A significant net sink for CO_2 in Tokyo Bay. Sci. Rep.,
836   7, 44355. https://doi.org/10.1038/srep44355.

837   54 Mehrbach, C., Cuberson, C. H., Hawley, J. E., and Pytkowicz, R. M. 1973. Measurements of
838   the apparent dissociation constants of carbonic acid in seawater at atmospheric pressure. Limnol.
839   Oceanog., 18, 897–907, 1973.

840   55 Martins, J., Silva, T., Fernandes, A., Massone, C., Carreira, R., 2016. Characterization of
841   particulate organic matter in a Guanabara Bay- coastal ocean transect using elemental , isotopic
842   and molecular markers. PANAMJAS, 11, 276–291.

843   56 Miller, J. D., Espie, G. S. Canvin, D. T., 1990. Physiological aspects of CO_2 and HCO_3
844   transport by cyanobacteria: A review. Can. J. Bot. 68: 1291–1302. https://doi.org/10.1139/b90-
845   165.

846   57 Miyajima, T., Miyajima, Y., Hanba, Y.T., Yoshii, K., Koitabashi, T., Wada, E., 1995.
847   Determining the stable isotope ratio of total dissolved inorganic carbon in lake water by
848   GC/C/IIRMS. Limnol. Oceanog. 40, 994–1000. https://doi.org/10.4319/lo.1995.40.5.0994.

849   58 Miyajima, T., Tsuboi, Y., Tanaka, Y., Koike, I.,2009. Export of inorganic carbon from two
850   Southeast Asian mangrove forests to adjacent estuaries as estimated by the stable isotope
851   composition of dissolved inorganic carbon. J. Geophys. Res. Biogeosciences, 114(1), 1–12.
852   https://doi.org/10.1029/2008JG000861.

853   59 Mook, W.G., Tan, F.C., 1991. Stable carbon isotopes in rivers and estuaries, in: Degens, E.T.,
854   Kempe, S., Richey, J.E. (Eds.), Biogeochemistry of Major World Rivers. John Wiley and Sons,
855   Chichester, UK, pp. 245-264.

856   60 Mook, W. G., 2001. Environmental Isotopes in the Hydrological Cycle. Principles and
857   Applications. UNESCO/ IAEA Series, Paris.

858   61 Phillips, D.L., Gregg, J.W., 2001. Uncertainty in source partitioning using stable isotopes.
859   Oecologia 127, 171-179. https://doi.org/10.1007/s004420000578.

860   62 Rau, G. H., Riebesell, U., Wolf-Gladrow, D., 1996. A model of photosynthetic C-13
861   fractionation by marine phytoplankton based on diffusive molecular CO_2 uptake. Mar. Ecol. Prog.
862   Ser. 133, 275–285.Rebello, A. L., Ponciano, C. R., Melges, L. H. 1988. Avaliação da

863 produtividade primaria e da disponibilidade de nutrientes na Baia de Guanabara. An. Acad. Bras.
864 Cienc., 60, 419–430.

865 63 Ribeiro, C., Kjerfve, B., 2002. Anthropogenic influence on the water quality in Guanabara
866 Bay, Rio de Janeiro, Brazil. Reg. Environ. Chang. 3, 13–19. http://dx.doi.org/10.1007/s10113-
867 001-0037-5.

868 64 Robbins, L. L., Hansen, M. E., Kleypas, J. A., Meylan. S. C., 2010. CO2 Calc: a user-friendly
869 seawater carbon calculator for Windows, Max OS X, and iOS (iPhone), U.S. Geological Survey
870 Open-File Report, 2010–1280, 1–17, available at: http://pubs. usgs.gov/of/2010/1280/.

871 65 Samanta, S., Dalai, T. K., Pattanaik, J. K., Rai, S. K., Mazumdar, A., 2015. Dissolved
872 inorganic carbon (DIC) and its $\delta^{13}C$ in the Ganga (Hooghly) River estuary, India: Evidence of
873 DIC generation via organic carbon degradation and carbonate dissolution. Geochim. Cosmochim.
874 Acta, 165, 226–248. https://doi.org/10.1016/j.gca.2015.05.040.

875 66 Siegenthaler, U. and K. O. Miinnich. 13C/12C fractionation during CO2 transfer from air to
876 sea. In Bolin, B., editor, SCOPE 16 - The Global Carbon Cycle, pages 249-257. Wiley & Sons,
877 New York, 1981.

878 67 Strickland, J. D. H., Parsons, T. R., 1972. A practical handbook of seawater analysis, 2nd ed.
879 Fisheries Research Board of Canada Bulletin.

880 68 Van Dam, B. R., Tobias, C., Holbach, A., Paerl, H. W. Zhu, G., 2018. CO2limited conditions
881 favor cyanobacteria in a hypereutrophic lake: An empirical and theoretical stable isotope study.
882 Limnol. Oceanogr. 63, 1643–1659. https://doi.org/10.1002/lno.10798.

883 69 Wang, X., Luo, C., Ge, T. Xu, C. Xue, Y., 2016. Controls on the sources and cycling of
884 dissolved inorganic carbon in the Changjiang and Huanghe River estuaries, China: ^{14}C and ^{13}C
885 studies. Limnol. Oceanogr. 61(4), 1358–1374. https://doi.org/10.1002/lno.10301

886 70 Yang X., Xue, L., Li, Y., Han, P., Liu, X., Zhang, L., Cai, W.-J., 2018. Treated Wastewater
887 Changes the Export of Dissolved Inorganic Carbon and Its Isotopic Composition and Leads to
888 Acidification in Coastal Oceans. Environ. Sci. Technol. 52, 5590–5599.
889 https://doi.org/10.1021/acs.est.8b00273.

890 71 Zeebe, R. E., Wolf-Gladrow, D., 2001. CO_2 in Seawater: Equilibrium, Kinetics, Isotopes.
891 Elsevier Oceanography Series, 65Amsterdam.

892 72 Zhang, J., P. D. Quay, and D. O. Wilbur (1995), Carbon isotope fractionation during gas-water
893 exchange and dissolution of CO_2, Geochim. Cosmochim. Acta, 59(1), 107–114,
894 doi:10.1016/0016-7037(95)91550-D.

Graphical Abstract

Source of CO_2 and DIC
^{13}C-depleted DIC

Phytoplankton blooms
Sink of CO_2 and DIC
^{13}C-enriched DIC